Abdominal Radiology (2019) 44:2346–2356
https://doi.org/10.1007/s00261-019-01995-4

HOLLOW ORGAN GI

Feasibility of using computed tomography texture analysis parameters as imaging biomarkers for predicting risk grade of gastrointestinal stromal tumors: comparison with visual inspection

In Young Choi[1] · Suk Keu Yeom[1] · Jaehyung Cha[2] · Sang Hoon Cha[1] · Seung Hwa Lee[1] · Hwan Hoon Chung[1] · Chang Min Lee[3] · Jungwoo Choi[4]

Published online: 28 March 2019

Abstract

Purpose To evaluate the feasibility of using computed tomography texture analysis (CTTA) parameters for predicting malignant risk grade and mitosis index of gastrointestinal stromal tumors (GISTs), compared with visual inspection.

Method and materials CTTA was performed on portal phase CT images of 145 surgically confirmed GISTs (mean size: 42.9 ± 37.5 mm), using TexRAD software. Mean, standard deviation, entropy, mean of positive pixels (MPP), skewness, and kurtosis of CTTA parameters, on spatial scaling factor (SSF), 2–6 were compared by risk grade, mitosis rate, and the presence or absence of necrosis on visual inspection. CTTA parameters were correlated with risk grade. Diagnostic performance was evaluated with receiver operating characteristic curve analysis. Enhancement pattern, necrosis, heterogeneity, calcification, growth pattern, and mucosal ulceration were subjectively evaluated by two observers.

Results Three to four parameters at different scales were significantly different according to the risk grade, mitosis rate, and the presence or absence of necrosis ($p < 0.041$). MPP at fine or medium scale ($r = -0.547$ to -393) and kurtosis at coarse scale (r = 0.424–0.454) correlated significantly with risk grade ($p < 0.001$). HG-GIST was best differentiated from LG-GIST by MPP at SSF 2 (AUC, 0.782), and kurtosis at SSF 4 (AUC, 0.779) (all $p < 0.001$). CT features predictive of HG-GIST were density lower than or equal to that of the erector spinae muscles on enhanced images (OR 2.1; $p = 0.037$; AUC, 0.59), necrosis (OR, 6.1; $p < 0.001$; AUC, 0.70), heterogeneity (OR, 4.3; $p < 0.001$; AUC, 0.67), and mucosal ulceration (OR, 3.3; $p = 0.002$; AUC, 0.62).

Conclusion Using TexRAD, MPP and kurtosis are feasible in predicting risk grade and mitosis index of GISTs. CTTA demonstrated meaningful accuracy in preoperative risk stratification of GISTs.

Keywords Computed tomography texture analysis · Gastrointestinal stromal tumor · Mitosis rate · Risk stratification

✉ Suk Keu Yeom
pagoda20@gmail.com

In Young Choi
ciy1114@naver.com

Jaehyung Cha
dolcha@korea.ac.kr

Sang Hoon Cha
sahcha@korea.ac.kr

Seung Hwa Lee
gareureung@daum.net

Hwan Hoon Chung
chungmic@korea.ac.kr

Chang Min Lee
korntera@hanmail.net

Jungwoo Choi
nausika@korea.ac.kr

[1] Department of Radiology, Korea University Ansan Hospital, Korea University College of Medicine, 123 Jeokgeum-ro, Danwon-gu, Ansan 15355, Republic of Korea

[2] Department of Biostatistics, Korea University Ansan Hospital, Korea University College of Medicine, 123 Jeokgeum-ro, Danwon-gu, Ansan 15355, Republic of Korea

[3] Department of Surgery, Korea University Ansan Hospital, Korea University College of Medicine, 123 Jeokgeum-ro, Danwon-gu, Ansan 15355, Republic of Korea

[4] Department of Pathology, Korea University Ansan Hospital, Korea University College of Medicine, 123 Jeokgeum-ro, Danwon-gu, Ansan 15355, Republic of Korea

Introduction

Gastrointestinal stromal tumors (GISTs) are the most common mesenchymal tumors of the gastrointestinal tract [1, 2]. About 10–30% of GISTs are clinically malignant, but all GISTs are considered to have some degree of malignant potential [2, 3]. The malignancy risk of GISTs is determined based on the mitotic index, tumor size, and site of the lesion according to National Comprehensive Cancer Network (NCCN) guidelines [4]. Imatinib mesylate, a 2-phenyl amino pyrimidine derivative that functions as a specific inhibitor of tyrosine kinase, is the treatment of choice after surgery for tumors with a high malignancy risk. It is also used post operatively to prevent tumor recurrence and metastasis [2]. The malignancy risk of tumor is confirmed histologically after surgery. Depending on this risk, a post-operative treatment plan is determined [3, 5]. In the NCCN guideline, if the size of the tumor is more than 10 cm or the mitosis count is more than 5 in high-power fields (HPFs), the gastric GIST is classified as a high risk. For tumors in the small and large intestines, if the tumor size exceeds 5 cm, or the mitosis count is more than 5 in 50 HPFs, the tumor is classified as a high risk [4].

The mitotic index is the key feature for assessing malignancy risk and is considered one of the most important prognostic factors for GISTs [2, 6, 7]. However, the mitotic index cannot be assessed without histological examination. Preoperative endoscopic biopsy of a mass is commonly performed but it has a risk of hemorrhage [8, 9]. Furthermore, a core-needle biopsy may be inconclusive if a necrotic or hemorrhagic portion of the tumor is sampled and has the limitation of sampling bias [10].

Contrast-enhanced computed tomography (CT) is the most commonly used imaging modality for diagnosing and staging GIST, because it can show well the tumor extent and its metastasis. CT texture analysis (CTTA) is a novel imaging postprocessing tool used to measure tissue heterogeneity that may not be perceptible to the naked eye. Texture analysis makes available an objective and quantitative evaluation of tumor heterogeneity by analyzing the distribution and relationship of pixel gray levels in the image [11]. Recently, several texture analysis software programs have become commercially available. These programs usually provide output on a variety of histogram characteristics including the mean and standard deviation (SD) of the attenuation, entropy, mean of positive pixels (MPP), skewness, and kurtosis of values, and can be used with various spatial scaling factors [12]. It is likely that these different factors can reveal microscopic histological features, such as necrosis, ischemia, fibrosis, vascularity, and histologic homogeneity, of regions of interest (ROIs). Recent studies have shown that CTTA can help to depict the types and histopathological grades of tumors in various organs [12, 13]. Many commercial texture analysis software programs have made CTTA analysis easier for researchers. Various studies have used texture analysis with these software programs to evaluate differential diagnosis, tumor grade stratification, prognosis, and treatment responses in various types of tumors [13–22]. Previous studies have shown that density heterogeneity in lung cancer, quantified by CTTA, may reflect necrotic and ischemic areas of the tumor [23]. High-grade tumors usually show a high mitotic index and high cellularity; malignant tumors more often present with high vascularity and heterogenous density due to the high incidence of internal hemorrhage and necrosis than do benign tumors [11]. We hypothesized that CTTA could provide quantitative information about the malignancy risk and mitotic count in GISTs. Therefore, the purpose of our study was to the evaluate feasibility of using CTTA parameters for predicting the malignancy risk and mitotic index of GISTs, in comparison with the visual inspection.

Materials and methods

Patients

Our institutional review board approved this retrospective study and waived the requirement for obtaining informed patient consent. Through a computerized search of medical records, we identified 312 patients who had histopathologically confirmed GIST in gastrointestinal tracts from August 2007 to August 2017. Of these patients, 168 patients were excluded for the following reasons: (1) no curative surgery was performed at our hospital ($n=89$), (2) no available contrast-enhanced CT images was obtained within 1 month before the surgery ($n=41$), (3) no visible tumor on CT images or tumor size less than 1 cm in diameter on images ($n=30$), (4) unacceptable CT image quality due to artifacts ($n=4$), and (5) insufficient pathologic data ($n=4$). The final study population included 144 patients (66 men and 78 women; mean age ± standard deviation [SD], 59.6 ± 12.4 years) with 145 GISTs (Fig. 1).

Patients underwent complete surgical resection. One pathologist with 15 years' experience reviewed all patients' pathology reports and the microscopic slides of the tumors and recorded mitosis count and histological grade of the tumors. The malignancy risk of GISTs was graded according to NCCN guidelines [10] (Table 1).

CT examinations

The CT images obtained on the date closest to the date of surgery were selected for the analysis; the mean interval

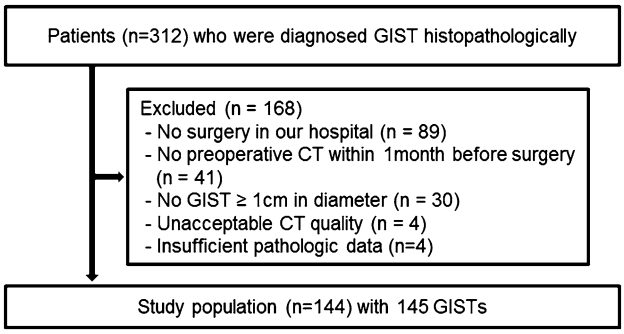

Fig. 1 Flowchart of the study population. CT, computed tomography; GIST, gastrointestinal stromal tumors

between preoperative CT and surgery was 13 ± 12 days. Measurements were performed using portal phase CT images. CT scans were performed using multidetector CT scanners (iQON, Brilliance iCT, Ingenuity, and Brilliance 64: Philips Healthcare and Medical Systems, USA and Netherland; Aquilion ONE: Toshiba, Minato, Japan) using the following parameters: tube potential of 100–120 kV and a matrix of 512 × 512 × 16. All CT scans were performed using automated tube potential, and the slice thickness used was 2–5 mm (Table 2).

Quantitative evaluation of CT images using texture analyses

All image measurements and texture analysis were performed by a single radiologist, with 8 years of experience in abdominal imaging interpretation who was blinded to the histological grade of the GISTs and using a high-resolution monitor on a picture archiving and communication system (INFINIT; Infinity, Seoul, South Korea). Texture analysis of all lesions was performed using commercial research software (TexRAD Ltd, Cambridge, UK). Identification of GISTs and selection of the representative section for placing the region of interest (ROI) were performed by consensus of two experienced abdominal radiologists. The two overall largest transverse diameters of each tumor were selected. Two-slice images were then analyzed using the commercially available texture analysis software program. ROIs were manually drawn to encompass as much of the lesion as possible on two consecutive slices of portal phase images, while leaving a 1-mm peripheral margin outside the ROI to avoid including air or fat. The parametric values from the two image sections were averaged, and the average was then used as a representative value (Fig. 2).

We performed texture analysis of the lesions with each filter setting, i.e., a built-in Laplacian of Gaussian spatial bandpass filter, including fine (spatial scaling factor [SSF] 2), medium (SSF 3–4), and coarse (SSF 5–6) filter settings (Fig. 2). We recorded texture analysis, parameters including the mean and standard deviation (SD) of gray-level intensity (mean), entropy, mean positive pixels (MPP), skewness, and kurtosis.

Table 2 Summary of CT acquisition protocol

		Number
Vendor		
	iQON	3
	iCT	5
	Ingenuity	50
	Brilliance 64	67
	Aquilion	20
Thickness (mm)		
	5	80
	3	9
	2	56
Scan delay time		
	60 s after bolus tracking	103
	90 s after contrast injection	42

Table 1 NCCN risk stratification of primary GISTs by Mitotic Index, size, and site

Mitotic Index (per 50 HPF)	Size (cm)	Gastric	Duodenum	Jejunum/Ileum	Rectum
≤ 5	≤ 2	None	None	None	None
	> 2, ≤ 5	Very low	Low	Low	Low
	> 5, ≤ 10	Low	Moderate	Insufficient data	Insufficient data
	> 10	Moderate	High	High	High
> 5	≤ 2	None	High	Insufficient data	High
	> 2, ≤ 5	Moderate	High	High	High
	> 5, ≤ 10	High	High	Insufficient data	Insufficient data
	> 10	High	High	High	High

NCCN National Comprehensive Cancer Network, *HPF* high-power field, *GISTs* gastrointestinal stromal tumors

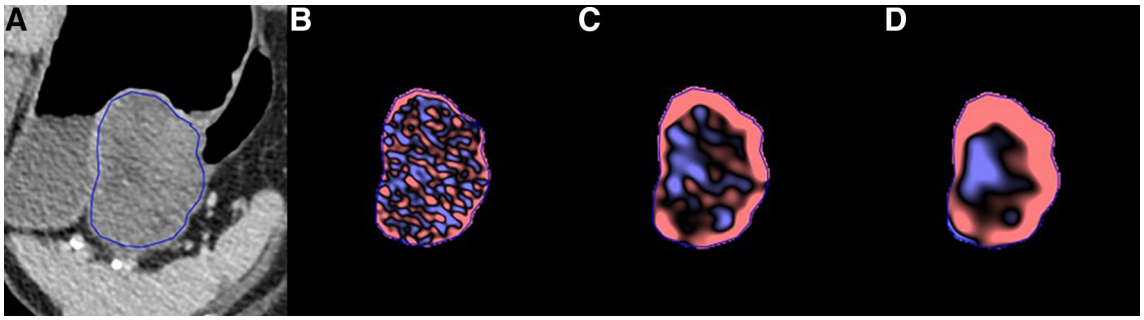

Fig. 2 Illustration of regions of interest and corresponding texture images at a texture scale of 2, 4, and 6. The portal phase image shows an exophytic, heterogenous low-density mass in the gastric body of a 73-year-old woman; the mass was histologically diagnosed as high-risk GIST after surgery. SSF, spatial scaling factor

Visual inspection of GIST on CT images

Two radiologists performed visual inspection of GIST findings. We evaluated the enhancement pattern (higher density than the erector spinae muscles in back, or not), necrosis (presence or absence of an area of less than 10 HU), heterogeneity (presence or absence), calcification (presence or absence), growth pattern (endo- or exoluminal), and mucosal ulceration (presence or absence) on a portal phase CT scan. Mucosal ulceration was defined as indentation or discontinuation of the enhancing inner layer on the luminal surface of the tumor [24]. Interobserver agreement between the two readers for each finding was calculated.

Statistical analyses

We evaluated the correlation between CTTA parameters including mean, SD, entropy, MPP, skewness, and kurtosis, according to each SSF (2, 3, 4, 5, and 6) and the malignancy risk grade of the tumor determined according to the NCCN guidelines, using Spearman's rank correlation test. The differences among CTTA parameters according to the risk grade were analyzed using ANOVA and post hoc analysis with Bonferroni adjustment for multiple comparisons.

We also analyzed the differences in CTTA parameters according to the mitosis index (>5, or ≤ 5) of the tumor and the absence or presence of necrosis on visual inspection using the Mann–Whitney test.

We categorized the five risk grades (no risk, very low risk, low risk, and moderate risk, and high risk) into two groups: LG-GIST, including no-, very low-, and low-risk grades and HG-GIST, including moderate- and high-risk grades.

The diagnostic performances of CTTA parameters in differentiating HG-GIST from LG-GIST were evaluated using receiver operating characteristics (ROC) curve analysis. The area under the ROC curve (AUC) for each parameter for diagnosing of HG-GIST was obtained, and the sensitivity and the specificity of each parameter were calculated at the optimal cutoff values determined by the largest Youden index.

All the CTTA parameters and CT features on visual inspection were independently tested in logistic regression analysis to evaluate their effects on the likelihood that a tumor would be classified as HG-GIST. Odds ratios (ORs) and empirical ROC curves were calculated with 95% confidence intervals (CIs).

Interobserver agreement of CT features on visual inspection was analyzed using kappa statistics. A kappa value of 0.20 or less indicated poor agreement; 0.21–0.40, fair agreement; 0.41–60, moderate agreement; 0.61–0.80 good agreement; and 0.81–1.00, excellent agreement.

Statistical analyses were performed using SPSS version 21.0 (IBM SPSS, Armonk, NY, USA) and MedCalc version 18.11 (MedCalc Software bvba, Ostend, Belgium). A p value of less than .05 was considered to indicate a significant difference.

Results

The mean tumor size was 42.9 ± 37.5 mm (range 10–240 mm). The 145 GISTs were stratified into 33 no-, 47 very low-, 13 low-, 20 moderate-, and 32 high-risk GISTs according to the NCCN guideline. Table 3 summarizes the characteristics of the lesions.

CTTA parameter distribution according to risk grade and mitosis rate

MPP at a fine or medium scale ($r = -0.547$ to -0.393) and kurtosis at a coarse scale ($r = 0.424$–0.454) correlated significantly with risk grade ($p < 0.001$).

Three parameters (mean, MPP, and kurtosis) at SSF 2, and four parameters (mean, SD, MPP, and kurtosis) at SSF 3, 4, 5, and 6 differed significantly according to the risk

Table 3 Summary of risk stratification of primary GIST lesions

Mitotic Index (per 50 HPF)	Size (cm)	Gastric	Duodenum	Jejunum/ Ileum	Rectum	Total
≤ 5	≤ 2	21	6	2	2	31
	> 2, ≤ 5	47	4	5	0	56
	> 5, ≤ 10	4	1	3	1	9
	> 10	2	1	1	0	4
> 5	≤ 2	2	0	0	0	2
	> 2, ≤ 5	14	4	2	0	20
	> 5, ≤ 10	8	0	5	0	13
	> 10	7	1	2	0	10
	Total	105	17	20	3	145

HPF high-power field, *GIST* gastrointestinal stromal tumor

grade ($p < 0.037$). Entropy and skewness did not show significant differences according to the risk grade at any SSF.

Four parameters (mean, SD, MPP, kurtosis) at SSF 2 and five parameters (mean, SD, MPP, skewness, kurtosis) at SSF 3, 4, 5, and 6 differed according to mitosis rate ($p < 0.041$). Entropy did not show significant differences at any scaling factor. Mean, SD, and MPP in GISTs with a high mitotic index were significantly lower than those in GISTs with a low mitotic index, at all SSFs. Skewness in GISTs with a high mitotic index was significantly higher than that GISTs with a low mitotic index, at SSF 3, 4, 5, and 6. Kurtosis in GISTs with a high mitotic index was significantly higher than that in GISTs with a low mitotic index, at SSF 4 and 5 (Table 4).

Diagnostic performance of CTTA parameters for differentiating of LG-GISTs from HG-GISTs

CTTA parameters are compared between LG-GISTs and HG-GISTs in Table 5. Mean and MPP in HG-GISTs were significantly lower than those in LG-GIST at all SSFs. Skewness and kurtosis in HG-GISTs were significantly higher than those in LG-GISTs, at all SSFs.

For the differentiation of HG-GIST from LG-GIST, MPP at SSF 2 showed the largest AUC (0.782), followed by kurtosis at SSF 4 (0.779) (all $p < 0.001$) (Fig. 3). At the optimal cutoff value of 49.3, MPP at SSF 2 yielded a sensitivity of 88.7% and a specificity of 59.8%, and at the optimal cutoff values of 0.26, kurtosis at SSF 4 yielded in a sensitivity of 71.7% and a specificity of 75%, for differentiating HG-GISTs from LG-GISTs.

On quantitative evaluation using CTTA parameters, MPP at SSF 2, kurtosis at SSF 4, and skewness at SSF 5 were significant factors. Diagnostic accuracy using logistic regression analysis of CTTA parameters was 78.6%. The OR and 95% Cis of MPP at SSF 2, kurtosis at SSF 4, and skewness at SSF 5 were 0.93 (0.89–0.96), 1.58 (1.09–2.27), and 3.39 (1.37–8.39), respectively.

Diagnostic performance of visual inspection parameters for differentiation of LG-GISTs and HG-GISTs

On subjective evaluation, density lower than or equal to that of the erector spinae muscles on enhanced images, presence of necrosis, heterogenous density, no calcification, an endoluminal growth pattern, and the presence of mucosal ulceration were significantly more common in HG-GIST than in LG-GISTs (Fig. 4). Table 6 shows the CT features according to the tumor grade. The CT features predictive of HG-GISTs were density lower than or equal to that of the erector spinae muscles on enhanced images (OR, 2.1; $p = 0.037$; AUC, 0.59), the presence of necrosis (OR, 6.1; $p < 0.001$; AUC, 0.70), heterogenous density (OR, 4.3; $p < 0.001$; AUC, 0.67), and the presence of mucosal ulceration (OR, 3.3; $p = 0.002$; AUC, 0.62).

Interobserver agreement of visual inspection parameters was excellent. More specifically, the interobserver agreement of enhancement pattern, necrosis, heterogeneity, presence of calcification, growth pattern, and mucosal ulceration between the two readers were 0.881, 0.862, 0.986, 0.959, 0.898, and 0.899, respectively ($p < 0.041$).

Comparison of CTTA parameter values with or without necrosis

Four parameters (mean, SD, MPP, kurtosis) at SSF 2, three parameters (mean, MPP, entropy, kurtosis) at SSF 3, 4, and three parameters (mean, MPP, kurtosis) at SSF 5, 6 differed according to the presence of necrosis on visual inspection ($p < 0.036$). Skewness did not show significant differences at any scaling factor. Mean and MPP in GISTs with necrosis were significantly lower than those in GISTs without necrosis on visual inspection, at all SSFs. Kurtosis in GISTs with necrosis was significantly higher than that in GISTs without necrosis on visual inspection at all SSFs. Entropy in GISTs

Table 4 CTTA parameters according to the mitosis rate

Filter size	Parameters	GISTs with low mitotic index ($n=100$)	GISTs with high mitotic index ($n=45$)	p value
SSF2				
	Mean	17.07 ± 19.18	5.74 ± 7.04	< 0.001
	SD	57.9 ± 14.9	48.06 ± 9.76	< 0.001
	MPP	53.25 ± 17.17	40.08 ± 9.70	< 0.001
	Skewness	0.033 ± 0.46	0.16 ± 0.32	0.056
	Kurtosis	0.68 ± 1.73	1.1 ± 1.88	0.205
SSF3				
	Mean	25.23 ± 29.68	8.04 ± 9.27	< 0.001
	SD	57.98 ± 17.85	45.60 ± 10.56	< 0.001
	MPP	58.67 ± 26.15	38.88 ± 10.1	< 0.001
	Skewness	− 0.05 ± 0.58	0.13 ± 0.41	0.032
	Kurtosis	0.55 ± 1.70	1.13 ± 1.83	0.075
SSF4				
	Mean	31.58 ± 38.70	9.62 ± 12.40	< 0.001
	SD	58.76 ± 21.0	45.38 ± 10.92	< 0.001
	MPP	63.94 ± 33.83	39.94 ± 11.45	< 0.001
	Skewness	− 0.11 ± 0.57	0.09 ± 0.45	0.030
	Kurtosis	0.26 ± 1.66	0.92 ± 1.59	0.024
SSF5				
	Mean	35.95 ± 45.36	10.62 ± 15.95	< 0.001
	SD	58.01 ± 2.44	48.91 ± 1.89	< 0.001
	MPP	67.30 ± 38.63	40.97 ± 13.06	< 0.001
	Skewness	− 0.14 ± 0.53	0.04 ± 0.43	0.032
	Kurtosis	0.07 ± 1.57	0.65 ± 1.40	0.030
SSF6				
	Mean	38.28 ± 50.02	11.13 ± 19.29	< 0.001
	SD	57.95 ± 23.44	45.66 ± 12.12	< 0.001
	MPP	68.81 ± 41.50	41.85 ± 14.4	< 0.001
	Skewness	− 0.14 ± 0.54	0.00 ± 0.42	0.021
	Kurtosis	− 0.27 ± 1.44	0.42 ± 1.25	0.062

Data are given as means ± standard deviations (SD)

MPP, mean of positive pixels; LG-GIST, includes no-risk, very low-risk, and low-risk grade GISTs; HG-GIST, includes moderate- and high-risk grade GISTs; GISTs, gastrointestinal stromal tumors; SSF, spatial scaling factor

with necrosis was significantly higher than that in GISTs without necrosis on visual inspection at SSF 3, 4.

Discussion

This study showed that CTTA parameters may be helpful in preoperative stratification of malignancy risk of GIST. We found that HG-GISTs were characterized by significantly lower mean, SD, and MPP, and higher skewness and kurtosis, compared with LG-GISTs. ROC analysis demonstrated that MPP at a fine SSF and kurtosis at a coarse SSF showed the highest diagnostic performance for differentiating HG-GISTs from LG-GISTs. These texture analysis parameters were superior to conventional parameters, such as mean density or SD, in the differential diagnosis of HG-GISTs and LG-GISTs. We found that GISTs with a high mitotic index were characterized by significantly lower mean, SD, and MPP, and higher skewness and kurtosis than those with low mitotic index, similarly to HG-GISTs. Texture analysis allowed us to obtain various objective indicators. These indices are expected to reflect the histological characteristics of the lesions. Numerous studies have reported that various texture analysis parameters are related to the degree of lesion malignancy. There are many useful texture parameters such as entropy, kurtosis, maximum frequency, and mean gray level intensity, in addition to size, mean density, and SD [4, 12, 13, 16, 19, 21, 23, 25]. It is a parameter that expresses the irregularity or complexity of CT density of the tissue and has been related to be a histological grade of many tumors

Table 5 CTTA parameters according to the risk grade

Filter size	Parameters	LG-GISTs ($n=92$)	HG-GISTs ($n=53$)	p value
SSF2				
	Mean	18.37 ± 2.02	5.20 ± 0.94	< 0.001
	SD	58.74 ± 1.55	48.09 ± 1.39	< 0.001
	MPP	54.64 ± 1.79	39.66 ± 1.79	< 0.001
	Skewness	0.0084 ± 0.047	0.18 ± 0.047	0.006
	Kurtosis	0.54 ± 1.64	1.14 ± 1.59	< 0.001
SSF3				
	Mean	26.80 ± 3.15	7.91 ± 1.35	< 0.001
	SD	58.20 ± 1.88	47.09 ± 1.63	< 0.001
	MPP	59.84 ± 2.78	39.84 ± 1.50	< 0.001
	Skewness	− 0.079 ± 0.057	0.16 ± 0.069	0.002
	Kurtosis	0.33 ± 0.15	1.43 ± 0.29	< 0.001
SSF4				
	Mean	33.24 ± 4.13	10.06 ± 1.79	< 0.001
	SD	58.40 ± 2.24	48.02 ± 1.81	0.001
	MPP	64.72 ± 3.64	42.21 ± 1.82	< 0.001
	Skewness	− 0.13 ± 0.05	0.10 ± 0.076	0.005
	Kurtosis	0.047 ± 0.0115	1.19 ± 0.296	< 0.001
SSF5				
	Mean	37.56 ± 4.87	11.65 ± 2.22	0.001
	SD	58.01 ± 2.44	48.91 ± 1.89	0.031
	MPP	67.68 ± 4.18	44.29 ± 2.07	< 0.001
	Skewness	− 0.16 ± 0.048	.042 ± 0.076	0.007
	Kurtosis	− 0.12 ± 0.09	0.89 ± 0.29	< 0.001
SSF6				
	Mean	39.171 ± 5.39	12.74 ± 2.64	0.002
	SD	56.81 ± 2.52	49.29 ± 14.3	0.136
	MPP	68.83 ± 4.52	45.88 ± 2.23	0.003
	Skewness	− 0.15 ± 0.05	0.0017 ± 0.075	0.021
	Kurtosis	− 0.19 ± 0.087	0.63 ± 0.26	0.000

Data are given as means ± standard deviations (SD)

CTTA, computed tomography texture analysis; MPP, mean of positive pixels; LG-GIST, includes no-risk, very low-risk, and low-risk grade GISTs; HG-GIST, includes moderate- and high-risk grade GISTs; GISTs, gastrointestinal stromal tumors; SSF, spatial scaling factor

including renal cell carcinoma, pancreatic cancer, neuroendocrine tumor, urothelial cancer, and lung cancer [12, 13, 16, 19, 21, 23]. Zhang et al. reported that entropy was significantly different between high-grade and low-grade urothelial carcinomas [13]. However, in this study, entropy did not show significant differences between HG-GISTs and LG-GISTs. The various texture parameters may have different significance depending on the type of tumor, the type of imaging study, and the method of analysis. Further studies are required to clarify the importance of the different parameters. In this situation, easy-to-use commercial programs can facilitate an objective evaluation of the usefulness of each parameter and confirm their use as imaging biomarkers for various tumors.

The malignancy of the GIST is determined by the location, size, and mitosis index of the tumor. Of these parameters, the mitosis index can only be confirmed by biopsy. If the mitosis index is high, the proliferation of the tissue is rapid, which results in increased complications such as hemorrhage, necrosis, infarction, and cystic change within the tissue. Therefore, it is plausible that necrosis and heterogeneity noted on visual inspection could be associated with an increased mitosis count, and our observations are generally reasonable. Previous studies have described necrosis in the tumor, heterogeneous tumor density, large tumor size (> 11 cm), and metastasis to the liver or peritoneum on CT images as findings suggesting high-grade GIST or a high mitotic index of the tumor [26–28]

To date, there has been no report of the differences in CTTA parameters according to the mitotic index. In the current study, ROC analysis demonstrated the highest diagnostic performance for differentiating GISTs with a high mitotic index from those with a low mitotic index for MPP at a fine SSF. MPP reduces the impact of dark objects on the mean histogram value [11]. HG-GISTs and GISTs with a high mitotic index showed smaller MPP values than LG-GISTs and GISTs with a low mitotic index. This may be due to the increased hypodense portion in HG-GISTs and GISTs with a high index count. Kurtosis is known to be inversely related to the number of objects highlighted and to reflect tumor heterogeneity. HG-GISTs showed a larger kurtosis than LG-GISTs; this may be due to increased tumor heterogeneity. The differences of CTTA parameters with or without necrosis on visual inspection also showed similar results with those according to the mitotic index. The GISTs with necrosis on visual inspection showed lower mean, MPP, higher kurtosis at all SSFs, and higher entropy at medium SSFs than those without necrosis on visual inspection. We thought that the lower values for MPP and mean represent the lower attenuation values seen at necrosis and the higher kurtosis suggesting a wider distribution of attenuation values which are seen as heterogenic areas in necrosis. These findings are consistent with other paper that previously analyzed the relationship between tumor necrosis and CTTA parameters [29].

A single study has reported on the correlations between texture parameters and malignancy risk of GISTs [4]. That report used in-house-produced software (Image analyzer 1.0, China) and showed that maximum frequency (the peak value of a histogram) from arterial phase images was superior to other parameters for indicating risk. We used parameters different from those used in that study; the parameters used in the present study have been common and widely used and validated in recent studies. We could not evaluate the maximum frequency because the

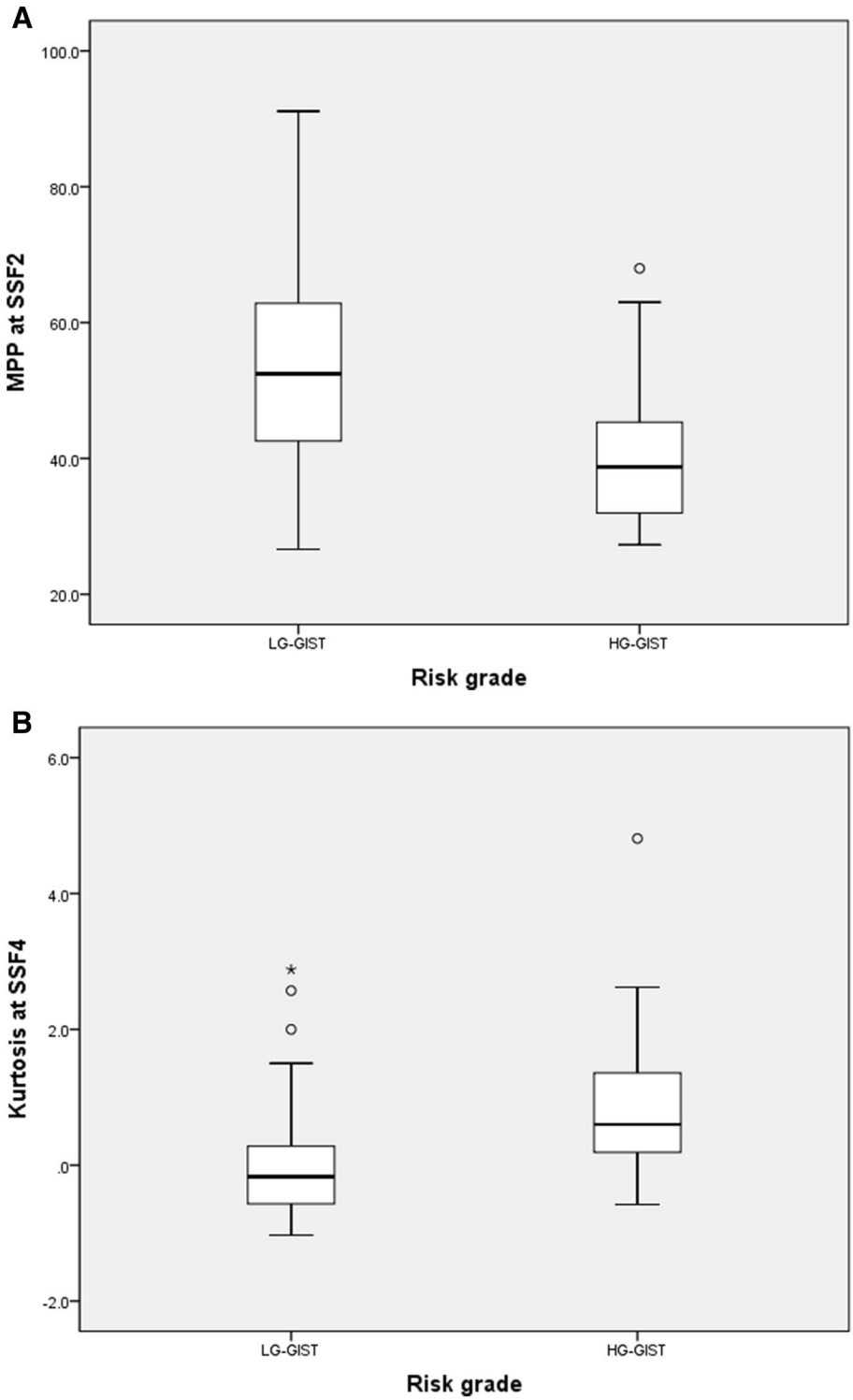

Fig. 3 Box plots summarizing MPP (**a**) and kurtosis (**b**) values of the GISTs. The top and bottoms of the boxes represent the first and third quartiles, respectively. The length of the box represents the interquartile range. Lines within each box are medians. Error bars show the highest or the lowest value within 1.5 times of the interquartile range of the upper or lower quartiles. Data points outside the box are outliers. *$p < 0.001$. MPP, mean of positive pixels; LG-GIST includes no-risk, very low-risk, and low-risk grade GISTs; HG-GIST includes moderate- and high-risk grade GISTs; GISTs, gastrointestinal stromal tumors

CT acquisition time was not uniform. The use of commercialized texture analysis software employing image filtering to show the differentiation of GISTs according to mitotic count has not been reported previously. The TexRAD software uses Laplacian of Gaussian bandpass filters of 2-D isotropic measures of the second spatial derivative of an image, which allows to alteration of the image pixel intensity patterns and extraction of specific structures corresponding to the width of filter [11]. This technique makes it possible to overcome the differences in images arising from using different CT protocols. Texture analysis using TexRAD can be retrospectively performed

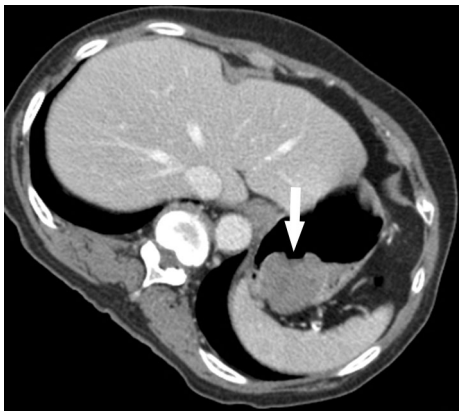

Fig. 4 Representative CT image in a 65-year-old man with a GIST. Axial CT image shows a 4.4-cm-sized, heterogenous enhancing mass in the gastric fundus. Axial CT image shows mucosal ulceration at the center portion of the mass. Coronal CT image shows a low attenuation portion in the mass. Two radiologists classified it as the mass with suspicious of necrosis. This mass showed 33.1 of mean of positive pixels (MPP) at spatial scaling factor (SSF) 2, and 1.32 of kurtosis at SSF 4. After resection, this mass presented high mitotic count, 51/50 high-power field. This mass was stratified as a high risk. *CT* computed tomography, *GIST* gastrointestinal stromal tumor

on data acquired using standard clinical imaging protocols and can be easily applied at any hospitals.

The differences in kurtosis according to risk grade and mitosis count was greater when using coarse filters, while the differences in MPP according to risk grade and mitosis count were greater when using fine filters. The filter size that best represents the histological characteristics of the tumor will depend on what we are looking at.

Although the diagnostic accuracy of the two methods cannot be compared statistically, the accuracy of differential diagnosis of HG-GISTs from LG-GISTs using CTTA parameters was similar to or slightly better than that of visual inspection. CTTA parameters have the advantage of providing objective and quantitative values as compared with visual evaluation. Visual inspection requires experience in radiology and may be subjective; however, texture analysis provides objective and quantitative information. Schieda et al. reported that quantitative texture analysis is more accurate than visual analysis when identifying the heterogeneity of sarcomatoid renal cell carcinomas as compared with clear cell renal cell carcinomas [30].

For treatment of GIST, except in cases where complete resection of the tumor is not possible or when metastasis is present, complete resection of tumor should be performed, and should be accomplished with a safe resection margin, intact pseudo-capsule, without rupture of the tumor, and without seeding of metastasis in the abdominal cavity during operation. The stability and usefulness of laparoscopic excision of GIST are known; however, for large tumors, care should be taken with laparoscopic excision because of the risk of rupture [31–34]. Primary chemotherapy of these tumors is ineffective, but neoadjuvant chemotherapy has been attempted to reduce the tumor to a size that is operable. In high-risk GIST, adjuvant chemotherapy with Imatinib should be used even after complete resection. In some cases, intermediate risk cases have also been given adjuvant chemotherapy to reduce the risk of metastasis and tumor recurrence [35]. For this reason, we included the moderate risk group in the HG-GIST category.

This study had several limitations. First, this study had a retrospective design, and there may have been selection bias. The study did not include malignant GISTs with metastasis or adjacent solid organ invasion, because the patients underwent surgery for complete resection. Second, there was some heterogeneity in the CT techniques used for our study because of its retrospective design. A previous study showed that CTTA using TexRAD is robust to differences in CT techniques, including slice thickness, tube current, and voltage [36]. It has denoising or gray-level standardization steps to help remove differences that arise for technical rather than biological reasons. Third, since ROIs for all cases were drawn based on consensus of two radiologists, interobserver agreement was not measured in this study. However,

Table 6 Summary of visual inspection results

Parameters	LG-GISTs ($n=93$)	HG-GISTs ($n=52$)	Odds ratio	Confidential interval	p value	Sensitivity	Specificity	AUC
Density lower than or equal to that of the back muscle	30 (32.3)	26 (50.0)	2.1	1.047–4.212	0.037	50	67.7	0.589
Necrosis	17 (18.3)	30 (57.7)	6.096	2.848–13.049	< 0.001	57.7	81.7	0.697
Heterogenous density	38 (40.9)	39 (75.0)	4.342	2.048–9.207	< 0.001	75	59.1	0.671
Calcification	10 (10.8)	3 (5.8)	0.508	0.133–1.936	0.321	5.8	89.2	0.475
Endoluminal growth	56 (60.2)	37 (71.2)	1.630	0.786–3.381	0.189	71.2	39.8	0.555
Mucosal ulceration	18 (19.4)	23 (44.2)	3.305	1.559–7.003	0.002	44.2	80.6	0.624

Data are shown as the numbers of tumors, with percentages in parentheses

LG-GIST includes no-risk, very low-risk, and low-risk grade GISTs; HG-GIST includes moderate- and high-risk grade GISTs; GISTs gastrointestinal stromal tumors

because the ROI was drawn to include entire tumor, the difference between the observers is expected to be small.

Second-order or high-order statistics parameters analyze texture in a specific direction using adjacent gray-tone difference matrices. Therefore they can examine location and relationships between three or more pixels, in addition to the first-order parameters provided by the TexRAD program [11]. These parameters are intended to represent more complex or delicate configurations of tissue texture and have shown good results in several studies [37–40].

In conclusions, CTTA parameters, such as MPP and kurtosis can be useful in predict the risk grade and mitosis index of GISTs. In our study, texture analysis parameters demonstrated meaningful accuracy in preoperative diagnosis of tumor risk stratification and can be used as imaging biomarkers for determination of tumor grade.

Acknowledgements This research was supported by a Korea University Ansan Hospital Grant (O1801331) and Korea University Grant (K1422331).

Compliance with ethical standards

Conflicts of interest The scientific guarantor of this publication is Suk Keu Yeom. The authors of this manuscript declare no relationships with any companies, whose products or services may be related to the subject matter of the article. The authors state that this work has not received any funding.

References

1. Hirota S, Isozaki K, Moriyama Y, Hashimoto K, Nishida T, Ishiguro S, Kawano K, Hanada M, Kurata A, Takeda M, Muhammad Tunio G, Matsuzawa Y, Kanakura Y, Shinomura Y, Kitamura Y (1998) Gain-of-function mutations of c-kit in human gastrointestinal stromal tumors. Science 279 (5350):577-580
2. Park CH, Kim GH, Lee BE, Song GA, Park DY, Choi KU, Kim DH, Jeon TY (2017) Two staging systems for gastrointestinal stromal tumors in the stomach: which is better? BMC gastroenterology 17 (1):141. https://doi.org/10.1186/s12876-017-0705-7
3. Sepe PS, Brugge WR (2009) A guide for the diagnosis and management of gastrointestinal stromal cell tumors. Nature reviews Gastroenterology & hepatology 6 (6):363-371. https://doi.org/10.1038/nrgastro.2009.43
4. Liu S, Pan X, Liu R, Zheng H, Chen L, Guan W, Wang H, Sun Y, Tang L, Guan Y, Ge Y, He J, Zhou Z (2018) Texture analysis of CT images in predicting malignancy risk of gastrointestinal stromal tumours. Clinical radiology 73 (3):266-274. https://doi.org/10.1016/j.crad.2017.09.003
5. Phongkitkarun S, Phaisanphrukkun C, Jatchavala J, Sirachainan E (2008) Assessment of gastrointestinal stromal tumors with computed tomography following treatment with imatinib mesylate. World journal of gastroenterology 14 (6):892-898
6. Miettinen M, Sobin LH, Lasota J (2005) Gastrointestinal stromal tumors of the stomach: a clinicopathologic, immunohistochemical, and molecular genetic study of 1765 cases with long-term follow-up. The American journal of surgical pathology 29 (1):52-68
7. Bertin M, Angriman I, Scarpa M, Mencarelli R, Ranzato R, Ruffolo C, Polese L, Iacobone M, D'Amico DF (2007) Prognosis of gastrointestinal stromal tumors. Hepato-gastroenterology 54 (73):124-128
8. Scarpa M, Bertin M, Ruffolo C, Polese L, D'Amico DF, Angriman I (2008) A systematic review on the clinical diagnosis of gastrointestinal stromal tumors. Journal of surgical oncology 98 (5):384-392. https://doi.org/10.1002/jso.21120
9. Eckardt AJ, Adler A, Gomes EM, Jenssen C, Siebert C, Gottschalk U, Koch M, Rocken C, Rosch T (2012) Endosonographic large-bore biopsy of gastric subepithelial tumors: a prospective multicenter study. European journal of gastroenterology & hepatology 24 (10):1135-1144. https://doi.org/10.1097/meg.0b013e328356eae2
10. Demetri GD, von Mehren M, Antonescu CR, DeMatteo RP, Ganjoo KN, Maki RG, Pisters PW, Raut CP, Riedel RF, Schuetze S, Sundar HM, Trent JC, Wayne JD (2010) NCCN Task Force report: update on the management of patients with gastrointestinal stromal tumors. Journal of the National Comprehensive Cancer Network : JNCCN 8 Suppl 2:S1-41; quiz S42-44
11. Lubner MG, Smith AD, Sandrasegaran K, Sahani DV, Pickhardt PJ (2017) CT Texture Analysis: Definitions, Applications, Biologic Correlates, and Challenges. Radiographics : a review publication of the Radiological Society of North America, Inc 37 (5):1483-1503. https://doi.org/10.1148/rg.2017170056
12. Lubner MG, Stabo N, Abel EJ, Del Rio AM, Pickhardt PJ (2016) CT Textural Analysis of Large Primary Renal Cell Carcinomas: Pretreatment Tumor Heterogeneity Correlates With Histologic Findings and Clinical Outcomes. AJR American journal of roentgenology 207 (1):96-105. https://doi.org/10.2214/ajr.15.15451
13. Zhang GM, Sun H, Shi B, Jin ZY, Xue HD (2017) Quantitative CT texture analysis for evaluating histologic grade of urothelial carcinoma. Abdominal radiology 42 (2):561-568. https://doi.org/10.1007/s00261-016-0897-2
14. Andersen MB, Harders SW, Ganeshan B, Thygesen J, Torp Madsen HH, Rasmussen F (2016) CT texture analysis can help differentiate between malignant and benign lymph nodes in the mediastinum in patients suspected for lung cancer. Acta radiologica 57 (6):669-676. https://doi.org/10.1177/0284185115598808
15. Skogen K, Schulz A, Dormagen JB, Ganeshan B, Helseth E, Server A (2016) Diagnostic performance of texture analysis on MRI in grading cerebral gliomas. European journal of radiology 85 (4):824-829. https://doi.org/10.1016/j.ejrad.2016.01.013
16. Haider MA, Vosough A, Khalvati F, Kiss A, Ganeshan B, Bjarnason GA (2017) CT texture analysis: a potential tool for prediction of survival in patients with metastatic clear cell carcinoma treated with sunitinib. Cancer imaging : the official publication of the International Cancer Imaging Society 17 (1):4. https://doi.org/10.1186/s40644-017-0106-8
17. Jalil O, Afaq A, Ganeshan B, Patel UB, Boone D, Endozo R, Groves A, Sizer B, Arulampalam T (2017) Magnetic resonance based texture parameters as potential imaging biomarkers for predicting long-term survival in locally advanced rectal cancer treated by chemoradiotherapy. Colorectal disease : the official journal of the Association of Coloproctology of Great Britain and Ireland 19 (4):349-362. https://doi.org/10.1111/codi.13496
18. Cannella R, Borhani AA, Minervini MI, Tsung A, Furlan A (2018) Evaluation of texture analysis for the differential diagnosis of focal nodular hyperplasia from hepatocellular adenoma on contrast-enhanced CT images. Abdominal radiology. https://doi.org/10.1007/s00261-018-1788-5
19. Digumarthy SR, Padole AM, Lo Gullo R, Singh R, Shepard JO, Kalra MK (2018) CT texture analysis of histologically proven benign and malignant lung lesions. Medicine 97 (26):e11172. https://doi.org/10.1097/md.0000000000011172
20. Frood R, Palkhi E, Barnfield M, Prestwich R, Vaidyanathan S, Scarsbrook A (2018) Can MR textural analysis improve the prediction of extracapsular nodal spread in patients with oral

cavity cancer? European radiology. https://doi.org/10.1007/s00330-018-5524-x
21. Sandrasegaran K, Lin Y, Asare-Sawiri M, Taiyini T, Tann M (2018) CT texture analysis of pancreatic cancer. European radiology. https://doi.org/10.1007/s00330-018-5662-1
22. Ytre-Hauge S, Dybvik JA, Lundervold A, Salvesen OO, Krakstad C, Fasmer KE, Werner HM, Ganeshan B, Hoivik E, Bjorge L, Trovik J, Haldorsen IS (2018) Preoperative tumor texture analysis on MRI predicts high-risk disease and reduced survival in endometrial cancer. Journal of magnetic resonance imaging : JMRI. https://doi.org/10.1002/jmri.26184
23. Ganeshan B, Goh V, Mandeville HC, Ng QS, Hoskin PJ, Miles KA (2013) Non-small cell lung cancer: histopathologic correlates for texture parameters at CT. Radiology 266 (1):326-336. https://doi.org/10.1148/radiol.12112428
24. Cai PQ, Lv XF, Tian L, Luo ZP, Mitteer RA, Jr., Fan Y, Wu YP (2015) CT Characterization of Duodenal Gastrointestinal Stromal Tumors. AJR American journal of roentgenology 204 (5):988-993. https://doi.org/10.2214/ajr.14.12870
25. Guo C, Zhuge X, Wang Z, Wang Q, Sun K, Feng Z, Chen X (2018) Textural analysis on contrast-enhanced CT in pancreatic neuroendocrine neoplasms: association with WHO grade. Abdominal radiology. https://doi.org/10.1007/s00261-018-1763-1
26. Maldonado FJ, Sheedy SP, Iyer VR, Hansel SL, Bruining DH, McCollough CH, Harmsen WS, Barlow JM, Fletcher JG (2018) Reproducible imaging features of biologically aggressive gastrointestinal stromal tumors of the small bowel. Abdominal radiology 43 (7):1567-1574. https://doi.org/10.1007/s00261-017-1370-6
27. Tateishi U, Hasegawa T, Satake M, Moriyama N (2003) Gastrointestinal stromal tumor. Correlation of computed tomography findings with tumor grade and mortality. Journal of computer assisted tomography 27 (5):792-798
28. Pinaikul S, Woodtichartpreecha P, Kanngurn S, Leelakiatpaiboon S (2014) 1189 Gastrointestinal stromal tumor (GIST): computed tomographic features and correlation of CT findings with histologic grade. Journal of the Medical Association of Thailand = Chotmaihet thangphaet 97 (11):1189-1198
29. Iannarelli A, Sacconi B, Tomei F, Anile M, Longo F, Bezzi M, Napoli A, Saba L, Anzidei M, D'Ovidio G, Scipione R, Catalano C (2018) Analysis of CT features and quantitative texture analysis in patients with thymic tumors: correlation with grading and staging. La Radiologia medica 123 (5):345-350. https://doi.org/10.1007/s11547-017-0845-4
30. Schieda N, Thornhill RE, Al-Subhi M, McInnes MD, Shabana WM, van der Pol CB, Flood TA (2015) Diagnosis of Sarcomatoid Renal Cell Carcinoma With CT: Evaluation by Qualitative Imaging Features and Texture Analysis. AJR American journal of roentgenology 204 (5):1013-1023. https://doi.org/10.2214/ajr.14.13279
31. Novitsky YW, Kercher KW, Sing RF, Heniford BT (2006) Long-term outcomes of laparoscopic resection of gastric gastrointestinal stromal tumors. Annals of surgery 243 (6):738-745; discussion 745-737. https://doi.org/10.1097/01.sla.0000219739.11758.27.
32. Matsuhashi N, Osada S, Yamaguchi K, Okumura N, Tanaka Y, Imai H, Sasaki Y, Nonaka K, Takahashi T, Futamura M, Yoshida K (2013) Long-term outcomes of treatment of gastric gastrointestinal stromal tumor by laparoscopic surgery: review of the literature and our experience. Hepato-gastroenterology 60 (128):2011-2015
33. Bischof DA, Kim Y, Dodson R, Carolina Jimenez M, Behman R, Cocieru A, Blazer DG, 3rd, Fisher SB, Squires MH, 3rd, Kooby DA, Maithel SK, Groeschl RT, Clark Gamblin T, Bauer TW, Karanicolas PJ, Law C, Quereshy FA, Pawlik TM (2014) Open versus minimally invasive resection of gastric GIST: a multi-institutional analysis of short- and long-term outcomes. Annals of surgical oncology 21 (9):2941-2948. https://doi.org/10.1245/s10434-014-3733-3
34. Otani Y, Furukawa T, Yoshida M, Saikawa Y, Wada N, Ueda M, Kubota T, Mukai M, Kameyama K, Sugino Y, Kumai K, Kitajima M (2006) Operative indications for relatively small (2-5 cm) gastrointestinal stromal tumor of the stomach based on analysis of 60 operated cases. Surgery 139 (4):484-492. https://doi.org/10.1016/j.surg.2005.08.011
35. Lopez RL, del Muro XG (2012) Management of localized gastrointestinal stromal tumors and adjuvant therapy with imatinib. Anti-cancer drugs 23 Suppl:S3-6. https://doi.org/10.1097/cad.0b013e3283559fab
36. Miles KA, Ganeshan B, Griffiths MR, Young RC, Chatwin CR (2009) Colorectal cancer: texture analysis of portal phase hepatic CT images as a potential marker of survival. Radiology 250 (2):444-452. https://doi.org/10.1148/radiol.2502071879
37. Bashir U, Siddique MM, McLean E, Goh V, Cook GJ (2016) Imaging Heterogeneity in Lung Cancer: Techniques, Applications, and Challenges. AJR American journal of roentgenology 207 (3):534-543. https://doi.org/10.2214/ajr.15.15864
38. Tsujikawa T, Rahman T, Yamamoto M, Yamada S, Tsuyoshi H, Kiyono Y, Kimura H, Yoshida Y, Okazawa H (2017) (18)F-FDG PET radiomics approaches: comparing and clustering features in cervical cancer. Annals of nuclear medicine 31 (9):678-685. https://doi.org/10.1007/s12149-017-1199-7
39. Khene ZE, Bensalah K, Largent A, Shariat S, Verhoest G, Peyronnet B, Acosta O, DeCrevoisier R, Mathieu R (2018) Role of quantitative computed tomography texture analysis in the prediction of adherent perinephric fat. World journal of urology 36 (10):1635-1642. https://doi.org/10.1007/s00345-018-2292-9
40. Tsujikawa T, Yamamoto M, Shono K, Yamada S, Tsuyoshi H, Kiyono Y, Kimura H, Okazawa H, Yoshida Y (2017) Assessment of intratumor heterogeneity in mesenchymal uterine tumor by an (18)F-FDG PET/CT texture analysis. Annals of nuclear medicine 31 (10):752-757.